Title

Phase separation and large deviations of lattice active matter

Journal

The Journal of Chemical Physics, 148(15)

ISSN

0021-9606

Authors

Whitelam, Stephen

Klymko, Katherine

Mandal, Dibyendu

Publication Date

2018-04-21

DOI

10.1063/1.5023403

Peer reviewed

Phase separation and large deviations of lattice active matter

Stephen Whitelam, Katherine Klymko, and Dibyendu Mandal

Citation: The Journal of Chemical Physics **148**, 154902 (2018); doi: 10.1063/1.5023403
View online: https://doi.org/10.1063/1.5023403
View Table of Contents: http://aip.scitation.org/toc/jcp/148/15
Published by the American Institute of Physics

Phase separation and large deviations of lattice active matter

Stephen Whitelam,[1,a)] Katherine Klymko,[2] and Dibyendu Mandal[3]
[1]*Molecular Foundry, Lawrence Berkeley National Laboratory, 1 Cyclotron Road, Berkeley, California 94720, USA*
[2]*Department of Chemistry, University of California at Berkeley, Berkeley, California 94720, USA*
[3]*Department of Physics, University of California at Berkeley, Berkeley, California 94720, USA*

(Received 23 January 2018; accepted 26 March 2018; published online 20 April 2018)

Off-lattice active Brownian particles form clusters and undergo phase separation even in the absence of attractions or velocity-alignment mechanisms. Arguments that explain this phenomenon appeal only to the ability of particles to move persistently in a direction that fluctuates, but existing lattice models of hard particles that account for this behavior do not exhibit phase separation. Here we present a lattice model of active matter that exhibits motility-induced phase separation in the absence of velocity alignment. Using direct and rare-event sampling of dynamical trajectories, we show that clustering and phase separation are accompanied by pronounced fluctuations of static and dynamic order parameters. This model provides a complement to off-lattice models for the study of motility-induced phase separation. *Published by AIP Publishing.* https://doi.org/10.1063/1.5023403

I. INTRODUCTION

Active matter refers to systems whose elements propel themselves by dissipating energy. Natural examples of active matter include bacteria; synthetic examples include suspensions of colloids that can catalyze chemical reactions on their surface.[1–16] Continuous dissipation of energy ensures that active matter is "far" from equilibrium and able to display complex behavior that includes the generation and rectification of large fluctuations;[2,17–24] anomalous interfacial properties;[25] and phase separation in the absence of interparticle attractions.[1,6,9,11,12,14,26–33] This latter phenomenon, known as motility-induced phase separation (MIPS), is similar in some respects to equilibrium gas-liquid phase separation, e.g., MIPS can be described by free-energy-like quantities,[1,5,9,14] and different in others, e.g., active clusters fluctuate more than passive ones[4,28,34] (and more generally, it may be difficult to define the concept of a nonequilibrium "phase"[35]).

To probe these connections at a fundamental level, it is natural to identify the simplest models that exhibit such phenomena. Lattice models enable us to identify the microscopic origin of emergent phenomena, and they can be simulated on larger scales than their off-lattice counterparts, so facilitating calculation of, e.g., critical exponents.[36–39] The Ising model is the simplest model that displays equilibrium phase separation.[38] The Katz-Lebowitz-Spohn driven lattice gas is the prototypical example of drive-induced phase separation.[40,41] For active matter, there exist lattice models of MIPS induced by velocity alignment.[6,27,42,43] However, lattice models that account only for volume exclusion and persistent motion exhibit cluster formation and coarsening but do not undergo macroscopic phase separation.[44,45]

Here we introduce a lattice model that exhibits MIPS, in the absence of velocity alignment, and so allows study of the phenomenon in the simplest possible setting. Our starting point is the observation that simple kinetic arguments used to describe MIPS in off-lattice models appeal only to the fact that active particles diffuse and move persistently in a direction that fluctuates.[9] We show that a lattice model of active matter that captures the essence of such motion indeed exhibits MIPS (see Fig. 1), but only if particles possess the ability to move in a direction other than that of their drift. MIPS occurs in a region of phase space analogous to where it occurs off lattice (Fig. 2). We also use a simple rare-event sampling method[46,47] to show that clustering and phase separation is accompanied by non-Gaussian fluctuations of a particular dynamic order parameter (Fig. 3). This model allows the study of MIPS in a simple setting and provides a complement to other models of the phenomenon.[1,6,9,11,12,14,26–33]

II. MODEL AND PHENOMENOLOGY

We consider a square lattice of size L^2 in two dimensions, on which live N hard particles. The particle density is $\phi = N/L^2$. We apply periodic boundaries in both directions. As shown in Fig. 1(a), particles $\alpha = 1, 2, \ldots, N$ possess a (unit) orientation vector $\boldsymbol{e}_\alpha$ that can point in the direction of any nearest-neighbor site. Particle α on site i moves to a vacant nearest-neighbor site j with rate v_+, v_-, or v_0, if $\boldsymbol{e}_\alpha \cdot \boldsymbol{r}_{ij} = +1, -1$, or 0, respectively, where $\boldsymbol{r}_{ij}$ is the unit vector pointing from site i to site j. Particles cannot move to an occupied site. A particle's orientation vector rotates $\pi/2$ clockwise with rate D_+ and $\pi/2$ counter-clockwise with rate D_-. The orientation of a particle is unaffected by the orientation of neighboring particles (c.f. Refs. 6, 27, and 43). We simulated collections of particles using a continuous-time Monte Carlo algorithm.[48] We choose any possible process with probability W/R, where W is the rate of the process and R is the sum of rates of all possible processes, and update time by an amount $1/R$ after each move. An isolated active lattice particle moves in a manner similar to that of

[a)]swhitelam@lbl.gov

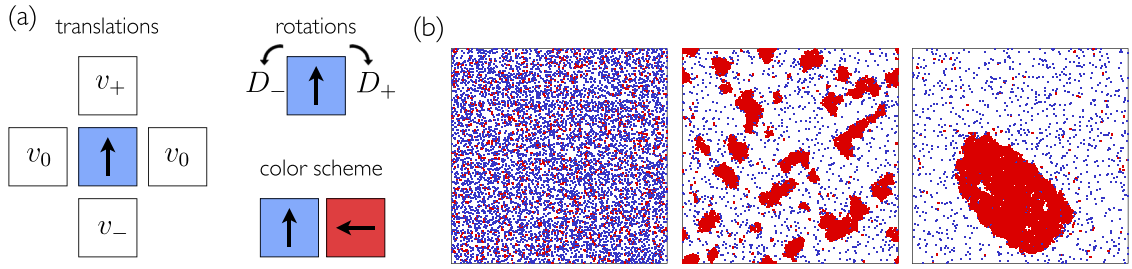

FIG. 1. (a) Rates for the motion of isolated lattice-based active particles (particles may not move to an occupied site), and the color scheme used in pictures: particles that point toward nearest-neighbor particles are shown in red, and those that do not are shown in blue. (b) Time-ordered configurations for density $\phi = 1/5$ and $v_+ = 25$, showing motility-induced phase separation. Lattice size is 200^2.

its off-lattice active Brownian counterpart (see Appendixes A and B)—both move ballistically on short scales and diffusively on large scales—and so we expect collections of such on-lattice particles to exhibit MIPS.

In Fig. 1(b), we show that this expectation is borne out. Randomly dispersed and oriented particles readily cluster and undergo phase separation, here via a spinodal decomposition-like mechanism involving the aggregation of many clusters (elsewhere in parameter space, we observe nucleation and growth of clusters). Similar in qualitative terms to their off-lattice counterparts,[9,28] clusters show pronounced fluctuations and transient internal voids; see Fig. 6 (Multimedia view). In this paper, we model unbiased rotational diffusion of the orientation vector ($D_+ = D_- \equiv D_{\rm rot} = 1/10$). In order to mimic positional diffusion that would occur off-lattice, we allow lateral and backward motion with some rate that is in general less than the drift rate (we set $v_- = v_0 = 1$). The presence of such motion is crucial. When $v_0 = v_- = 0$, i.e., when particles can move only in the direction of alignment, phase separation does not occur[44,45] (see Fig. 7). Two particles that meet head-on cannot move until one of them rotates. When jammed in this way they cannot merge with larger clusters in order to drive phase separation. This effect does not occur in off-lattice models or experiment, where two agents that meet head-on can slip past each other (by rectifying each other's motion). In other words, lattice-based active particles that cannot move against their orientation vector experience an unphysical kinetic trap that prevents MIPS (an exception is the model of Ref. 26, which achieves phase separation on-lattice by using a coarse-grained density field, effectively allowing particles to pass through each other). Introduction of local diffusion (nonzero v_-, v_0) removes this trap. Thus, in the absence of velocity alignment, MIPS on-lattice is achieved by a combination of volume exclusion, persistent motion, and local diffusive motion.

In Fig. 2, we show in a space of density ϕ and the rate v_+ for forward motion where MIPS occurs. As a simple measure of clustering we use f_4, the fraction of particles with 4 neighbors. Figure 2 shows the mean $\langle f_4 \rangle$ and log-variance $\ln(\langle f_4^2 \rangle - \langle f_4 \rangle^2)$ of this quantity from single simulations begun from disordered initial conditions [we defined averages of a microstate-dependent quantity $Q(C)$ as $\langle Q \rangle = \sum_k Q(C_k) R(C_k)^{-1} / \sum_k R(C_k)^{-1}$, where k labels microstates and $1/R(C)$ is the mean time taken to escape microstate C]. The region in which phase separation occurs can be roughly predicted by a flux-balance argument (see Appendix C) similar to that used off-lattice[9] (a more refined estimate of the position of the binodal could be made using the hydrodynamic approach used in Ref. 42). From this, we estimate that a fraction

$$f = \frac{{\rm Pe}\,\kappa - 1/\phi}{{\rm Pe}\,\kappa - 1} \tag{1}$$

of particles will be in the dense phase, where $4\kappa \equiv 1 - (1 - 2D_{\rm rot}/\Sigma)^{2\Sigma/D_{\rm rot}}$; $\Sigma \equiv v_+ + v_- + 2v_0 + 2D_{\rm rot}$; and the Péclet number ${\rm Pe} \equiv (v_+ - v_-)/(2D_{\rm rot})$ [for the parameters used, we have ${\rm Pe} = 5(v_+ - 1)$]. In Fig. 2, we plot the line $f = 1/2$. This line matches approximately the curvature of the phase boundary obtained by computer simulation, confirming that MIPS on-lattice occurs for a density-dependent Péclet number, as it does off lattice.[9] In addition, the variance of f_4 is large even in the ordered phase, indicating pronounced fluctuations of clusters (which is the case off lattice[28]).

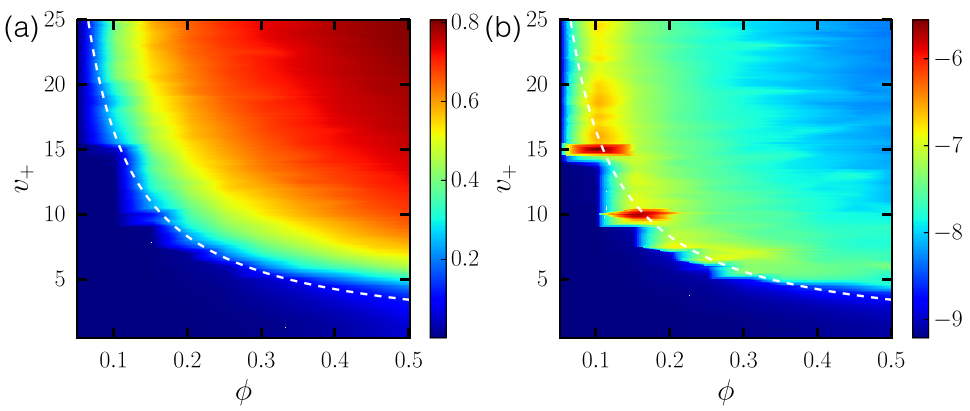

FIG. 2. (a) Mean and (b) logarithm of the variance of f_4, the fraction of particles with 4 neighbors, as a function of density ϕ and v_+ [the Péclet number ${\rm Pe} = 5(v_+ - 1)$]. As in the off-lattice model of Ref. 9, we observe phase separation at a density-dependent value of Pe. The dotted white line is the contour $f = 1/2$ from Eq. (1). Lattice size is 100^2.

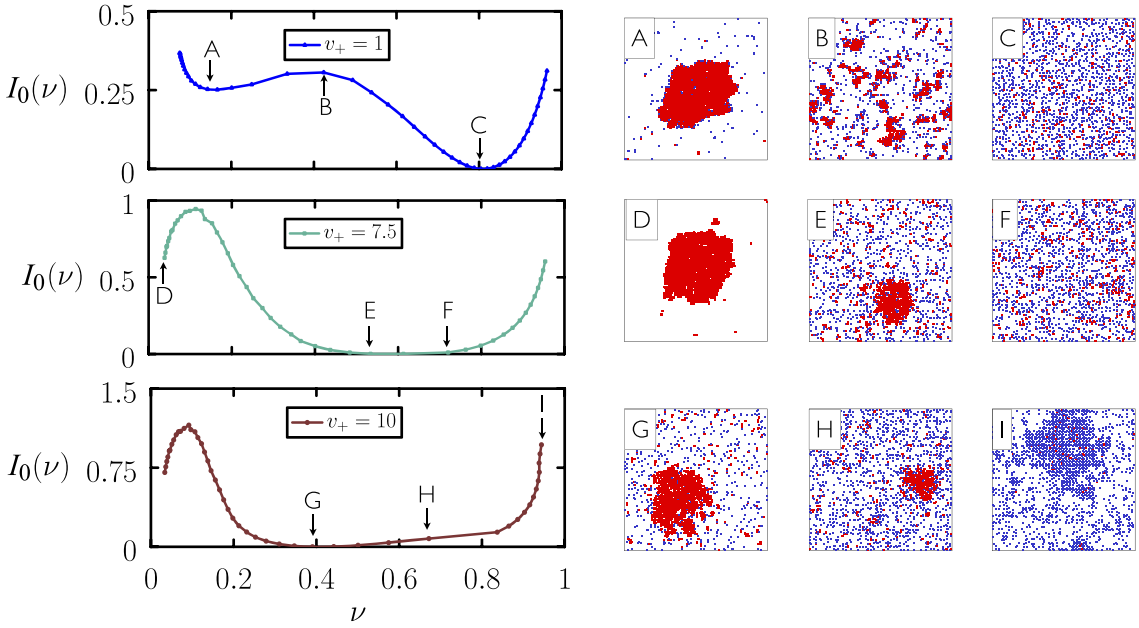

FIG. 3. Trajectory sampling yields an upper bound $I_0(\nu)$ on the large-deviation rate function for trajectory activity ν. Typical behavior is signaled by the vanishing of the rate function, while rare behavior corresponds to large values of the rate function. As we vary v_+, we change typical trajectories from being more active (large ν, top) to being less active (small ν, bottom). The MIPS transition occurs near the parameter set of the middle panel; see Fig. 2. Configurations from some typical and rare trajectories are shown in panels (A)–(I). Lattice size is 100^2, and density is $\phi = 1/5$.

III. TRAJECTORY SAMPLING

A. General considerations

To more thoroughly probe the fluctuations associated with clustering and phase separation, we used a simple method of rare-event sampling.[46,47] The method is motivated by the "thermodynamics of trajectories" or "s-ensemble" formalism[49–53] but is implemented differently; it could be considered a form of nonequilibrium umbrella sampling. Briefly, we wish to calculate $\rho(a, K)$, the probability distribution, over an ensemble of trajectories, of a quantity $a = A/K$. Here A is an observable extensive in the length of the trajectory and K is the number of simulation steps (configuration changes) in each trajectory in the ensemble. We define a trajectory as a sequence $\boldsymbol{x} = \{C_1, C_2, \ldots, C_K\}$ of microstates C_k visited by the dynamics. The probability of a step $C_k \to C_{k+1}$ in this sequence is $W(C_k \to C_{k+1})/R(C_k)$, where $W(C_k \to C_{k+1})$ is the rate for the enacted process, and $R(C_k) \equiv \sum_{C'} W(C_k \to C')$ is the sum of rates of all processes leading out of state C_k. Direct simulation of the model allows for efficient sampling of $\rho(a, K)$ for typical values of a and poor sampling of $\rho(a, K)$ for rare values of a. We therefore make use of a "change of measure"[54–60] and introduce a reference model whose rates

$$W_{\rm ref}(C \to C') = {\rm e}^{-s\alpha(C\to C')} W(C \to C') \tag{2}$$

are chosen so that the reference model's typical values of a are generated with low probability by the original model. Here $\alpha(C \to C')$ is the change of A upon moving from C to C', and s is a parameter. If $P[\boldsymbol{x}]$ and $P_{\rm ref}[\boldsymbol{x}]$ are the probabilities of generating a trajectory $\boldsymbol{x}$ using the original and reference models, respectively, then the ratio $w[\boldsymbol{x}] = P[\boldsymbol{x}]/P_{\rm ref}[\boldsymbol{x}]$ is

$$w[\boldsymbol{x}] = e^{sA[\boldsymbol{x}]+Kq[\boldsymbol{x}]}, \tag{3}$$

where

$$q[\boldsymbol{x}] \equiv K^{-1} \sum_{k=0}^{K-1} \ln \frac{R_{\rm ref}(C_k)}{R(C_k)}, \tag{4}$$

and $R_{\rm ref}(C_k) \equiv \sum_{C'} W_{\rm ref}(C_k \to C')$. The quantity we want, the probability density of a over trajectories of length K, is

$$\begin{aligned} \rho(a, K) &= \sum_{\boldsymbol{x}} P[\boldsymbol{x}] \delta(A[\boldsymbol{x}] - Ka) \\ &\equiv \sum_{\boldsymbol{x}} P_{\rm ref}[\boldsymbol{x}] w[\boldsymbol{x}] \delta(A[\boldsymbol{x}] - Ka) \\ &= {\rm e}^{sKa} \sum_{\boldsymbol{x}} P_{\rm ref}[\boldsymbol{x}] {\rm e}^{Kq[\boldsymbol{x}]} \delta(A[\boldsymbol{x}] - Ka). \end{aligned} \tag{5}$$

The probability distribution $\rho(a, K)$ is a reweighted version of the reference-model probability distribution $\rho_{\rm ref}(a, K) \equiv \sum_{\boldsymbol{x}} P_{\rm ref}[\boldsymbol{x}] \delta(A[\boldsymbol{x}] - Ka)$, which can be seen by writing (5) as

$$\begin{aligned} \rho(a, K) &= \rho_{\rm ref}(a, K) {\rm e}^{sKa} \frac{\sum_{\boldsymbol{x}} P_{\rm ref}[\boldsymbol{x}] {\rm e}^{Kq[\boldsymbol{x}]} \delta(A[\boldsymbol{x}] - Ka)}{\sum_{\boldsymbol{x}} P_{\rm ref}[\boldsymbol{x}] \delta(A[\boldsymbol{x}] - Ka)} \\ &\equiv \rho_{\rm ref}(a, K) {\rm e}^{sKa} \langle {\rm e}^{Kq[\boldsymbol{x}]} \rangle_a. \end{aligned} \tag{6}$$

Taking logarithms gives

$$I(a) = I_{\rm ref}(a) - sa - K^{-1} \ln \langle {\rm e}^{Kq[\boldsymbol{x}]} \rangle_a, \tag{7}$$

where $I(a) \equiv -K^{-1} \ln \rho(a, K)$ is the large-deviation rate function, for the original model, for the dynamic observable a.[54] $I_{\rm ref}(a)$ is the equivalent quantity for the reference model. Simulations of the reference model produce values of a that concentrate on a_s, where $I_{\rm ref}(a_s) = 0$, and so

$$I(a_s) = -sa_s - K^{-1} \ln \langle {\rm e}^{Kq[\boldsymbol{x}]} \rangle_{a_s}. \tag{8}$$

Simulations of the reference model, for given s, allow the two terms on the right-hand side of (8) to be estimated and therefore furnish one value $I(a_s)$ of the rate function of the original model. By repeating the process for a range of values of s, one can reconstruct the curve $I(a)$. In this sense, the rate function of

the reference model, $I_{\rm ref}(a)$, can be considered to be a nonequilibrium "umbrella potential" whose purpose is to concentrate sampling at a particular value of a.

The average in Eq. (8) can be evaluated by determining the statistics of $q[\boldsymbol{x}]$ for a set of typical reference-model trajectories (those for which $A[\boldsymbol{x}] = Ka_s$).[46,47] For models (such as the present one) that possess well-defined steady-state measures, one can obtain a bound $I_0(a) > I(a)$ on the rate function from individual trajectories of the reference model.[47] Applying Jensen's inequality to Eq. (8) gives

$$I(a_s) < I_0(a_s) = -sa_s - K^{-1} \ln \mathrm{e}^{K\langle q[\boldsymbol{x}]\rangle_{a_s}} = -sa_s - \sum_C \pi_{\rm ref}(C) \ln \frac{R_{\rm ref}(C)}{R(C)}, \quad (9)$$

where $a_s = A_s/K$ is a value of a typical of the reference model, and $\pi_{\rm ref}(C)$ is the steady-state probability of visitation, by the reference model, of state C. For a given value of s, Eq. (9) yields one point $I_0(a_s)$ on the curve $I_0(a)$; repeating the procedure for several values of s gives the whole curve.

B. Sampling trajectories of active particles

We next choose a dynamic observable a whose rate-function bound $I_0(a) > I(a)$ we wish to calculate. We choose a guided by studies of glasses. There, authors often choose to count the number of events that occur in a particular time, with the average time taken to leave configuration C being $1/R(C)$. This choice allows the identification of phase transitions out of equilibrium.[52,53,61] Similar physics should be accessible by measuring the values of $R(C)$ of states explored by a fixed number of configuration changes. We therefore take the reference-model bias $\alpha(C \to C') = B(C')$, where $B(C') = R(C')$ is the escape rate from the state to which the model is moving (we use B to emphasize that this choice can be varied); the order parameter against which dynamics are conditioned is $A/K = K^{-1} \sum_{k=0}^{K-1} B(C_{k+1})$, the mean relaxation rate of configurations comprising the trajectory (hereafter called the "activity" of the trajectory[52]). The reference model (2) is then

$$W_{\rm ref}(C \to C') = \mathrm{e}^{-sB(C')} W(C \to C'). \quad (10)$$

We simulate it as we do the original model, but now choosing events $C \to C'$ with probabilities $W_{\rm ref}(C \to C')/R_{\rm ref}(C)$. One can guide the reference model toward quickly or slowly relaxing configurations by varying the sign and magnitude of s. We compute (9) by running a single reference-model trajectory, for a given value of s, and evaluating the expression

$$I_0(a_s) = -sK^{-1} \sum_{k=0}^{K-1} [B(C_{k+1}) - B(C_k)] - K^{-1} \sum_{k=0}^{K-1} \ln \frac{\sum_{C'} \mathrm{e}^{-s[B(C')-B(C_k)]} W(C_k \to C')}{\sum_{C'} W(C_k \to C')}, \quad (11)$$

note that we have written $\ln \sum_{C'} \mathrm{e}^{-sB(C')} \equiv sB(C) + \ln \sum_{C'} \mathrm{e}^{-s[B(C')-B(C)]}$ so that numbers appearing in exponentials are not too large. The first term on the right-hand side of (11) becomes negligible for large K.

The reference model is a tool whose purpose is to tell us with what probability the original model will yield (rare) values of an observable. At the same time, configurations of the reference model indicate the nature of the configurations that will be visited, with low probability, by the original model. The reference model satisfies the relation $W_{\rm ref}(C \to C')/W_{\rm ref}(C' \to C) = \mathrm{e}^{-s[B(C')-B(C)]} W(C \to C')/W(C' \to C)$. Given that $B = R$ counts the numbers and types of particle-vacancy contacts, it is clear that biasing the system toward quickly ($s > 0$) or slowly relaxing ($s < 0$) configurations is akin to equipping particles with (anisotropic) repulsions or attractions, respectively. In the case $v_+ = v_- = v_0$, the original model comprises a set of diffusive hard particles, and the reference model, which measures the number of particle-vacancy bonds, is the Ising lattice gas with particle-particle interaction energy $-s$. Rare, slowly relaxing configurations of the original model therefore look like typical lattice gas configurations in the presence of an attractive interaction—i.e., they can be phase-separated—and rare, quickly relaxing configurations of the original model look like typical configurations of the lattice gas in the presence of repulsive interactions (which for certain particle densities are periodic and so hyperuniform[62]).

In Fig. 3, we show $I_0(\nu)$, an upper bound on the rate function associated with the (scaled) activity $\nu \equiv (\Sigma NK)^{-1} \sum_{k=0}^{K-1} B(C_k)$ (here N is the number of particles). To make this figure, we ran single reference-model trajectories of length $K = \mathcal{O}(10^8)$ for several values of s, both positive and negative. For each trajectory (prepared by starting with a single cluster and running until we entered steady state), we evaluated a ($=\nu N\Sigma$) and $I_0(a)$, using Eq. (11). Large values of ν correspond to active trajectories, i.e., those whose configurations change rapidly. Typical behavior is signaled by $I = 0$, while atypical behavior corresponds to large values of I. See Fig. 6 of Ref. 54 for an illustration of the relationship between a rate function and the associated probability density.

We see that increasing v_+ changes the typical behavior of the system (where the rate function vanishes) from being more active (top) to being less active (bottom). The snapshots (right) show that activity (ν) and clustering are largely anticorrelated: active trajectories generally contain configurations that are disordered, while less-active trajectories display clustered configurations.[63] However, activity (ν) and clustering are not perfectly correlated: for instance, there exist rare, active trajectories that exhibit "checkerboard" clustering. The curvature of the rate functions about their minima indicates the nature of near-typical fluctuations. For non-propelled particles (top), small fluctuations of ν are Gaussian, i.e., the rate function is quadratic about its minimum. Near the MIPS transition (middle panel), fluctuations become non-Gaussian, similar to the behavior of equilibrium systems near a phase boundary.[37] Note, however, that substantial non-Gaussian fluctuations persist into the region of phase separation (bottom panel). Non-Gaussian fluctuations of a different order parameter, cluster size, are seen in off-lattice models of active matter.[28]

The non-monotonic behavior seen in the rate functions indicates a change in the atypical behavior of trajectories as a function of s, the field conjugate to ν.[47] Trajectories conditioned upon certain values of ν can contain configurations very different to those observed in typical trajectories, e.g., rare configurations can be clustered while typical ones are disordered (top panels). Thus by varying v_+, we observe the MIPS transition at the level of typical trajectories (note the position

of the minima of the rate functions in the figure), while by varying s (conditioning against different ν), we can observe changes at the level of atypical trajectories (note the configurations associated with large values of the rate functions). A related scenario is seen in model lattice proteins[64] using the "s-ensemble" method of rare-event sampling.

IV. CONCLUSIONS

We have presented an on-lattice model of hard active particles that exhibits MIPS in the absence of velocity alignment. The model exhibits clustering and phase separation qualitatively similar to that seen in off-lattice models. Both direct simulations and trajectory-sampling methods show that pronounced fluctuations are present even within the ordered phase of the system. Lattice models provide a simple complement to off-lattice models, and the one presented here provides a simple way of studying motility-induced phase separation in the absence of velocity alignment.

ACKNOWLEDGMENTS

We thank Michael Hagan and Juan Garrahan for discussions. S.W. performed work at the Molecular Foundry, Lawrence Berkeley National Laboratory, supported by the Office of Science, Office of Basic Energy Sciences, of the U.S. Department of Energy under Contract No. DE-AC02–05CH11231. K.K. acknowledges support from an NSF Graduate Research Fellowship. D.M. acknowledges financial support by the U.S. Army Research Laboratory and the U.S. Army Research Office under Contract No. W911NF-13-1-0390.

APPENDIX A: MOTION OF AN ISOLATED OFF-LATTICE ACTIVE BROWNIAN PARTICLE

In this section, we recall some features of the typical motion of an isolated off-lattice two-dimensional active Brownian particle, of the type considered in some simulation studies.[9,28] In Appendix B, we show that an on-lattice active particle moves in a qualitatively similar way. The situation and notation considered in this section draws upon Sec. 4.3.1 of Ref. 8 (although it is not identical to the situation considered there); more comprehensive treatments of active-particle motion can be found elsewhere.[8,65,66]

1. Preliminaries

Consider numerical integration of the position of an active Brownian particle in $d = 2$. The particle is subject to thermal fluctuations and able to move deterministically in the direction of its orientation vector. After step N of the simulation, its position vector is $\boldsymbol{R}_N = \sum_{i=1}^{N} \Delta \boldsymbol{r}_i$, where

$$\Delta \boldsymbol{r}_i = \ell_0 \left(\cos\theta_{i-1}\hat{\boldsymbol{x}} + \sin\theta_{i-1}\hat{\boldsymbol{y}}\right) + \sqrt{2\Delta\tau D_x}\eta_i^x\hat{\boldsymbol{x}} + \sqrt{2\Delta\tau D_y}\eta_i^y\hat{\boldsymbol{y}}. \tag{A1}$$

Here $\hat{\boldsymbol{x}}$ and $\hat{\boldsymbol{y}}$ are Cartesian unit vectors; $\ell_0 = V_0\Delta\tau$ is the displacement magnitude of the deterministic force; $\Delta\tau$ is the integration time step; D_x and D_y are diffusion constants; θ_{i-1} is the angle (after step $i-1$ and before step i) between the particle's orientation vector and the x-axis; and η_i^x and η_i^y are Gaussian white noise terms with zero mean and unit variance, i.e., $\langle \eta_i^\alpha \rangle = 0$ and $\langle \eta_i^\alpha \eta_j^\beta \rangle = \delta_{\alpha,\beta}\delta_{i,j}$.

Let the particle angle evolve according to

$$\theta_i = \theta_{i-1} + \eta_i, \tag{A2}$$

where η_i is drawn from an even distribution $P(\eta_i)$. Let this distribution be bounded by $\pm\pi$ and have zero mean, in which case $\langle \sin\eta_i \rangle = 0$ and $\lambda \equiv \langle \cos\eta_i \rangle \neq 0$ (in general). We assume that angular changes at different times are uncorrelated.

For the sake of generality we shall consider three cases. The first is that of *driven matter* (see, e.g., Refs. 40 and 67), where the particle's orientation vector does not rotate. In this case $P(\eta_i) = \delta(\eta_i)$ and $\lambda = 1$. The second case is that of *active matter*, in which the particle's orientation angle rotates diffusively. In this case, we have $0 < \lambda < 1$. For the particular case of a Gaussian distribution $P(\eta_i)$, we have

$$\lambda = \int_{-\pi}^{\pi} \mathrm{d}\eta \cos\eta \cdot \frac{1}{\sqrt{2\pi\sigma^2}} \exp\left(-\frac{\eta^2}{2\sigma^2}\right) \approx \mathrm{e}^{-\sigma^2/2}, \tag{A3}$$

for σ small enough that the limits of the integral can be approximated by $\pm\infty$ (the exact solution can be written in terms of the error function). The third case is that of *Brownian matter*, where $P(\eta_i)$ is drawn uniformly from the interval $[-\pi, \pi)$. In this case $\lambda = 0$ (here the particle moves diffusively, with a diffusion constant renormalized by the drift parameter; see, e.g., Ref. 68).

To work out properties of the particle's motion, we will need

$$\begin{aligned}\langle \cos\theta_i \rangle &= \langle \cos(\theta_{i-1} + \eta_i) \rangle \\ &= \langle \cos\theta_{i-1} \rangle \langle \cos\eta_i \rangle - \langle \sin\theta_{i-1} \rangle \langle \sin\eta_i \rangle \\ &= \langle \cos\theta_{i-1} \rangle \lambda,\end{aligned} \tag{A4}$$

using the fact that noise terms at different times are uncorrelated. Equation (A4) is a recursion relation and implies

$$\langle \cos\theta_i \rangle = \cos\theta_0 \lambda^i, \tag{A5}$$

where θ_0 is the particle's initial angle. Similarly, $\langle \sin\theta_i \rangle = \sin\theta_0\lambda^i$.

To compute second moments of position, we need to average

$$\begin{aligned}&\Delta \boldsymbol{r}_i \cdot \Delta \boldsymbol{r}_j \\ &= \left(\ell_0 \cos\theta_{i-1} + \sqrt{2\Delta\tau D_x}\eta_i^x\right)\left(\ell_0 \cos\theta_{j-1} + \sqrt{2\Delta\tau D_x}\eta_j^x\right) \\ &\quad + \left(\ell_0 \sin\theta_{i-1} + \sqrt{2\Delta\tau D_y}\eta_i^y\right)\left(\ell_0 \sin\theta_{j-1} + \sqrt{2\Delta\tau D_y}\eta_j^y\right).\end{aligned} \tag{A6}$$

Anything linear in η^x or η^y will not survive the averaging; what remains to be averaged is

$$\ell_0^2 \cos(\theta_{j-1} - \theta_{i-1}) + 2\Delta\tau D_x \eta_i^x \eta_j^x + 2\Delta\tau D_y \eta_i^y \eta_j^y. \tag{A7}$$

For $i = j$, we have

$$\langle \Delta \boldsymbol{r}_i \cdot \Delta \boldsymbol{r}_i \rangle = \ell_0^2 + 2(\Delta\tau D_x + \Delta\tau D_y). \tag{A8}$$

For $j > i$, we have

$$\begin{aligned}\langle \Delta \boldsymbol{r}_i \cdot \Delta \boldsymbol{r}_j \rangle &= \ell_0^2 \langle \cos(\theta_{j-1} - \theta_{i-1}) \rangle \\ &= \ell_0^2 \lambda^{j-i}.\end{aligned} \tag{A9}$$

2. Character of motion

The position of the particle after step N is $\boldsymbol{R}_N = \sum_{i=1}^{N} \Delta \boldsymbol{r}_i$, and so

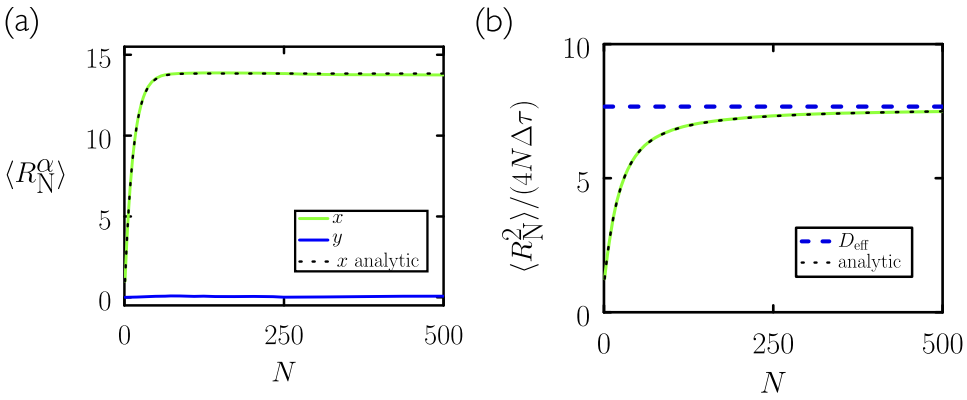

FIG. 4. Numerical integration of Eqs. (A1) and (A2) confirms the analytic results derived here, for (a) mean displacement (for $\alpha = x, y$) and (b) mean-squared displacement. The black dotted lines are analytic results (A14) and (A15); the blue dashed line $D_{\rm eff}$ is the result (A18). Here $V_0 = D_x = D_y = \Delta\tau = 1$, and $\sigma^2 = 0.15$, which gives $\lambda \approx 0.93$. Numerical averages are taken over 10^6 trajectories of a particle initially at the origin and oriented in the x-direction.

$$\langle \boldsymbol{R}_N \rangle = \sum_{i=1}^{N} \langle \Delta \boldsymbol{r}_i \rangle$$
$$= \ell_0 (\cos\theta_0 \hat{\boldsymbol{x}} + \sin\theta_0 \hat{\boldsymbol{y}}) \sum_{i=1}^{N} \lambda^{i-1} \quad \text{(A10)}$$
$$= \ell_0 \boldsymbol{e}_0 \frac{1-\lambda^N}{1-\lambda}, \quad \text{(A11)}$$

where $\mathrm{e}_0 \equiv \cos\theta_0 \hat{\boldsymbol{x}} + \sin\theta_0 \hat{\boldsymbol{y}}$ is the initial orientation vector of the particle. Here the angle brackets denote an average over trajectories (i.e., noise), for particles that start at the origin with angle θ_0.

For $\lambda \lesssim 1$ and N small, we can write $\lambda^N \approx 1 + N \ln\lambda$, in which case

$$\langle \boldsymbol{R}_N \rangle \approx N \ell_0 \boldsymbol{e}_0 \frac{(-\ln\lambda)}{1-\lambda}, \quad \text{(A12)}$$

i.e., on small scales, the particle moves ballistically. For large N, the mean displacement does not vanish but tends instead to the limit

$$\langle \boldsymbol{R}_\infty \rangle = \ell_0 \boldsymbol{e}_0 \frac{1}{1-\lambda}. \quad \text{(A13)}$$

Thus drift on short times generates a net displacement that is "remembered" by the particle at long times. Only if we average over initial orientations $\boldsymbol{e}_0$ does the net displacement vanish.

Results for the case of driven matter ($\lambda = 1$) and Brownian matter ($\lambda = 0$) can be obtained straightforwardly from (A11). Collecting these results, we have

$$\langle \boldsymbol{R}_N \rangle = \ell_0 \mathrm{e}_0 \times \begin{cases} N & (\lambda = 1) \\ \frac{1-\lambda^N}{1-\lambda} & (0 < \lambda < 1) \\ 0 & (\lambda = 0), \end{cases} \quad \text{(A14)}$$

for off-lattice driven, active, and Brownian matter, respectively.

The noise-averaged mean-squared displacement is

$$\langle \boldsymbol{R}_N \cdot \boldsymbol{R}_N \rangle = \langle \sum_{i=1}^{N} \Delta \boldsymbol{r}_i \cdot \sum_{i=j}^{N} \Delta \boldsymbol{r}_j \rangle$$
$$= \sum_{i=1}^{N} \langle \Delta \boldsymbol{r}_i \cdot \Delta \boldsymbol{r}_i \rangle + 2 \sum_{i=1}^{N-1} \sum_{j=i+1}^{N} \langle \Delta \boldsymbol{r}_i \cdot \Delta \boldsymbol{r}_j \rangle$$
$$= N\ell_0^2 + 2N(\Delta\tau D_x + \Delta\tau D_y) + 2\ell_0^2 \sum_{i=1}^{N-1} \sum_{j=i+1}^{N} \lambda^{j-i}$$
$$= N\ell_0^2 + 2N(\Delta\tau D_x + \Delta\tau D_y)$$
$$+ 2\ell_0^2 \frac{\lambda}{(1-\lambda)^2} (N(1-\lambda) - 1 + \lambda^N). \quad \text{(A15)}$$

In the case of active matter, we have ballistic motion on small scales, when $\lambda^N \approx 1$,

$$\langle \boldsymbol{R}_N \cdot \boldsymbol{R}_N \rangle \approx \ell_0^2 N^2 + 2N(\Delta\tau D_x + \Delta\tau D_y). \quad \text{(A16)}$$

We have diffusive motion on large scales (when $N \to \infty$), with an effective diffusion constant

$$D_{\rm eff} \equiv \lim_{N\to\infty} \frac{1}{4N\Delta\tau} \langle \boldsymbol{R}_N \cdot \boldsymbol{R}_N \rangle \quad \text{(A17)}$$
$$= \frac{\ell_0^2}{4\Delta\tau} \frac{1+\lambda}{1-\lambda} + \frac{1}{2}(D_x + D_y), \quad \text{(A18)}$$

which is renormalized by the self-propulsion of the particle.

Collecting results we have

$$\langle \boldsymbol{R}_N \cdot \boldsymbol{R}_N \rangle = \begin{cases} N^2\ell_0^2 + 2N(\Delta\tau D_x + \Delta\tau D_y) & (\lambda = 1) \\ \text{Eq. (A15)} & (0 < \lambda < 1) \\ N\ell_0^2 + 2N(\Delta\tau D_x + \Delta\tau D_y) & (\lambda = 0), \end{cases}$$

for off-lattice driven, active, and Brownian matter, respectively.

In Fig. 4, we confirm these analytic results numerically: an active Brownian particle moves ballistically at short times, possesses a mean displacement that is non-vanishing, and is effectively diffusive at long times.

APPENDIX B: MOTION OF AN ISOLATED ON-LATTICE ACTIVE BROWNIAN PARTICLE

In this section, we show that the motion of an isolated lattice-based active particle is similar to that of the off-lattice particle of Appendix A.

1. Preliminaries

Consider an isolated on-lattice active Brownian particle of the type described in the main text, evolved using a continuous-time Monte Carlo algorithm. After step N of a simulation, the particle's position vector is $\boldsymbol{R}_N = \sum_{i=1}^{N} \Delta \boldsymbol{r}_i$, where

$$\Delta \boldsymbol{r}_i = (p_1(i) - p_4(i)) \cos\theta_{i-1} \hat{\boldsymbol{x}} + (p_3(i) - p_2(i)) \sin\theta_{i-1} \hat{\boldsymbol{x}}$$
$$+ (p_1(i) - p_4(i)) \sin\theta_{i-1} \hat{\boldsymbol{y}} + (p_2(i) - p_3(i)) \cos\theta_{i-1} \hat{\boldsymbol{y}}. \quad \text{(B1)}$$

Here $\theta_{i-1} \in \{0, \pi/2, \pi, 3\pi/2\}$ is the orientation angle of the particle immediately prior to step i. The functions $p_\alpha(i)$ have the following properties: $p_1(i)$ is 1 if $0 < \xi_i \le v_+/\Sigma$ and 0 otherwise, where ξ_i is a random variable uniformly distributed on (0, 1] and $\Sigma \equiv v_+ + 2v_0 + v_- + 2D_{\rm rot}$ is the total rate for all

the processes accessible to an isolated particle. Similarly, $p_2(i)$ is 1 if $v_+/\Sigma < \xi_i \le (v_+ + v_0)/\Sigma$ and 0 otherwise; $p_3(i)$ is 1 if $(v_+ + v_0)/\Sigma < \xi_i \le (v_+ + 2v_0)/\Sigma$ and 0 otherwise; and $p_4(i)$ is 1 if $(v_+ + 2v_0)/\Sigma < \xi_i \le (v_+ + 2v_0 + v_-)/\Sigma$ and 0 otherwise.

The angular degree of freedom θ evolves according to $\theta_i = \theta_{i-1} + \Delta\theta_i$, where

$$\Delta\theta_i = p_5(i)\frac{\pi}{2} - p_6(i)\frac{\pi}{2}. \tag{B2}$$

Here $p_5(i)$ is 1 if $(v_+ + 2v_0 + v_-)/\Sigma < \xi_i \le (v_+ + 2v_0 + v_- + D_{\rm rot})/\Sigma$ and 0 otherwise, and $p_6(i)$ is 1 if $(v_+ + 2v_0 + v_- + D_{\rm rot})/\Sigma < \xi_i \le 1$ and 0 otherwise.

Noise terms are different times uncorrelated and so averages $\langle\cdot\rangle$ over noise for trajectories of N total steps are given by $\prod_{i=1}^{N}\int_0^1 {\rm d}\xi_i(\cdot)$. We then have $\langle p_1(i)\cos\theta_{i-1}\rangle = \langle p_1(i)\rangle\langle\cos\theta_{i-1}\rangle$, etc. We also have

$$\begin{aligned}\langle\cos\theta_i\rangle &= \langle\cos(\theta_{i-1} + \Delta\theta_i)\rangle \\ &= \langle\cos\theta_{i-1}\rangle\langle\cos\Delta\theta_i\rangle - \langle\sin\theta_{i-1}\rangle\langle\sin\Delta\theta_i\rangle \\ &= \langle\cos\theta_{i-1}\rangle\lambda,\end{aligned} \tag{B3}$$

where $\lambda \equiv 1 - 2D_{\rm rot}/\Sigma$ (note that λ in the equations of Appendix A is distinct). The recursion relation (B3) implies $\langle\cos\theta_i\rangle = \cos\theta_0\lambda^i$, where θ_0 is the initial angle of the particle. Similarly, we have $\langle\sin\theta_i\rangle = \sin\theta_0\lambda^i$.

We then have

$$\langle\Delta\boldsymbol{r}_i\rangle = \frac{v_+ - v_-}{\Sigma}{\rm e}_0\lambda^{i-1} \equiv \ell_0{\rm e}_0\lambda^{i-1}, \tag{B4}$$

where $\boldsymbol{e}_0 \equiv (\cos\theta_0, \sin\theta_0)$ is the initial orientation vector of the particle. We have defined $\ell_0 \equiv (v_+ - v_-)/\Sigma$ (note that ℓ_0 in the equations of Appendix A are distinct). Finally,

$$\begin{aligned}\langle\Delta\boldsymbol{r}_i\cdot\Delta\boldsymbol{r}_i\rangle &= \langle(p_2(i) - p_3(i))^2 + (p_1(i) - p_4(i))^2\rangle \\ &= \frac{v_+ + 2v_0 + v_-}{\Sigma},\end{aligned} \tag{B5}$$

and, for $j > i$,

$$\langle\Delta\boldsymbol{r}_i\cdot\Delta\boldsymbol{r}_j\rangle = \langle p_1(j) - p_4(j)\rangle \times \langle(p_1(i) - p_4(i))\cos(\theta_{j-1} - \theta_{i-1})\rangle \tag{B6}$$

$$= \ell_0^2\lambda^{j-i-1}. \tag{B7}$$

2. Character of motion

Using the results of Appendix B 1, we have

$$\langle\boldsymbol{R}_N\rangle = \sum_{i=1}^{N}\langle\Delta\boldsymbol{r}_i\rangle = \frac{v_+ - v_-}{\Sigma}\boldsymbol{e}_0\frac{1-\lambda^N}{1-\lambda}, \tag{B8}$$

for $0 < \lambda < 1$. Recall that $\lambda \equiv 1 - 2D_{\rm rot}/\Sigma$. Thus

$$\langle\boldsymbol{R}_N\rangle = \ell_0{\rm e}_0 \times \begin{cases} N & (\lambda = 1) \\ \dfrac{1-\lambda^N}{1-\lambda} & (0 < \lambda < 1) \\ 0 & (\lambda = 0), \end{cases} \tag{B9}$$

for on-lattice driven, active, and Brownian matter, respectively [driven matter corresponds to $D_{\rm rot} = 0$; Brownian matter corresponds to $\ell_0 = 0$, where $\ell_0 \equiv (v_+ - v_-)/\Sigma$]. For active matter, we have ballistic motion for small N,

$$\langle\boldsymbol{R}_N\rangle \approx N\ell_0\boldsymbol{e}_0\frac{(-\ln\lambda)}{1-\lambda}, \tag{B10}$$

and long-time non-vanishing mean displacement,

$$\langle\boldsymbol{R}_\infty\rangle = \ell_0\boldsymbol{e}_0\frac{1}{1-\lambda} \equiv \frac{v_+ - v_-}{2D_{\rm rot}}\boldsymbol{e}_0, \tag{B11}$$

similar to the off-lattice result (A13). This result suggests defining the Péclet number ${\rm Pe} \equiv (v_+ - v_-)/(2D_{\rm rot})$ so that $\langle\boldsymbol{R}_\infty\rangle = {\rm Pe}\,\boldsymbol{e}_0$.

The mean-squared displacement for $0 < \lambda < 1$ reads

$$\begin{aligned}\langle\boldsymbol{R}_N\cdot\boldsymbol{R}_N\rangle &= \langle\sum_{i=1}^{N}\Delta\boldsymbol{r}_i\cdot\sum_{i=j}^{N}\Delta\boldsymbol{r}_j\rangle \\ &= \sum_{i=1}^{N}\langle\Delta\boldsymbol{r}_i\cdot\Delta\boldsymbol{r}_i\rangle + 2\sum_{i=1}^{N-1}\sum_{j=i+1}^{N}\langle\Delta\boldsymbol{r}_i\cdot\Delta\boldsymbol{r}_j\rangle \\ &= N\frac{v_+ + 2v_0 + v_-}{\Sigma} \\ &\quad + 2\ell_0^2\frac{1}{(1-\lambda)^2}(N(1-\lambda) - 1 + \lambda^N),\end{aligned} \tag{B12}$$

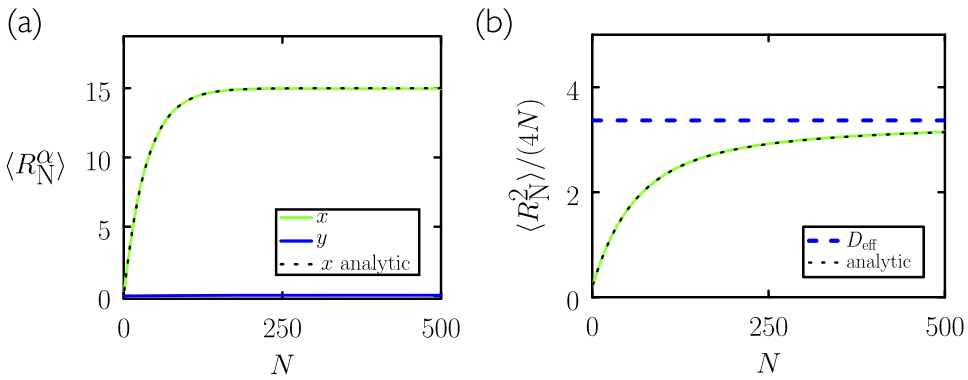

FIG. 5. Numerical evolution of an on-lattice active particle confirms the analytic results derived here, for (a) mean displacement (for $\alpha = x, y$) and (b) mean-squared displacement. The black dotted lines are analytic results (B9) and (B12); the blue dashed line $D_{\rm eff}$ is the result (B14). Here $v_+ = 4$, $v_- = v_0 = 1$, and $D_+ = D_- = 0.1$. Numerical averages are taken over 10^6 trajectories of a particle initially at the origin and oriented in the x-direction. The qualitative similarity between this figure and Fig. 4 emphasizes that isolated on-lattice and off-lattice active Brownian particles move in a similar fashion.

implying a long-time effective diffusivity

$$D_{\rm eff} \equiv \lim_{N\to\infty} \frac{1}{4N}\langle \boldsymbol{R}_N \cdot \boldsymbol{R}_N\rangle \tag{B13}$$

$$= \frac{1}{4}\frac{v_+ + 2v_0 + v_-}{\Sigma} + \frac{\ell_0^2}{2}\frac{1}{1-\lambda}. \tag{B14}$$

Thus an isolated active on-lattice Brownian particle behaves in a similar way to its off-lattice counterpart: it moves ballistically at short times, possesses a mean net displacement that is non-vanishing, and is effectively diffusive at long times.

Collecting results for all three cases, we have

$$\langle \boldsymbol{R}_N \cdot \boldsymbol{R}_N\rangle = \begin{cases} N(N-1)\ell_0^2 + N(v_+ + 2v_0 + v_-)/\Sigma & (\lambda = 1) \\ \text{Eq. (B12)} & (0 < \lambda < 1) \\ N(v_+ + 2v_0 + v_-)/\Sigma & (\lambda = 0), \end{cases} \tag{B15}$$

for on-lattice driven, active, and Brownian matter, respectively.

In Fig. 5, we confirm these analytic results numerically: an on-lattice active Brownian particle moves ballistically at short times, possesses a mean net displacement that is non-vanishing, and is effectively diffusive at long times, just like its off-lattice counterpart.

APPENDIX C: FLUX-BALANCE ARGUMENT TO ESTIMATE ONSET OF PHASE SEPARATION

To estimate when phase separation should occur on lattice, we construct a kinetic-theory argument, following the argument used in Ref. 9 to predict phase separation in an off-lattice model of active matter. Consider a simulation box containing a dense phase of density (number of particles per unit area) $\phi_{\rm d}$ and a gas of density $\phi_{\rm g}$. Consider a planar interface between these two phases and focus on the net rate of departure and arrival of particles, at the interface, due to the persistent component of particle motion. We ignore the diffusive component of particle motion because diffusion alone does not cause clusters to form.

Departure—Particles arriving at the interface will initially point into the dense phase. In order to leave, they must rotate so that they point in the opposite direction. The characteristic number of steps required for a particle to point in the direction opposite its arrival is $k = 2\sum_{m=1}^{\infty} m\,2^{-m} = 4$. The number of particles leaving the interface in this interval is $N_{\rm off} \sim l_{\rm int} \times \phi_{\rm d}$ (for $v + \gg D_{\rm rot}$), where $l_{\rm int}$ is the length of the interface.

Addition—The characteristic number of steps made by an isolated particle, as a trapped particle makes a single rotational step, is $\Sigma/(2D_{\rm rot}) \equiv 1/(1-\lambda)$. Thus an isolated particle makes $S = k/(1-\lambda)$ steps in the characteristic time taken for a trapped particle to become free. From the results of Appendix B 1, only those isolated particles within a distance $|\langle \boldsymbol{R}_S\rangle| = \ell_0(1-\lambda^S)/(1-\lambda)$ can reach the interface in S steps [recall that $\ell_0 \equiv (v_+ - v_-)/\Sigma$]. We then estimate that $N_{\rm on}$ is

$$N_{\rm on} \sim \frac{\phi_{\rm g}}{4} \times l_{\rm int} \times \ell_0 \frac{1-\lambda^S}{1-\lambda}. \tag{C1}$$

The factor of 1/4 comes from the fact that only 1/4 of particles will, on average, point toward the interface.

Flux balance—Equating $N_{\rm off}$ and $N_{\rm on}$, we get

$$\frac{\phi_{\rm d}}{\phi_{\rm g}} = \frac{v_+ - v_-}{8D_{\rm rot}}(1-\lambda^{k/(1-\lambda)}). \tag{C2}$$

This relation contains the drift velocity of the particle and its rotational diffusion constant. As in Appendix A, it is natural to define the Péclet number

$$\mathrm{Pe} \equiv \frac{v_+ - v_-}{2D_{\rm rot}}. \tag{C3}$$

We also define $\kappa \equiv (1-\lambda^{k/(1-\lambda)})/4$, in which case (C2) reads

$$\frac{\phi_{\rm d}}{\phi_{\rm g}} = \mathrm{Pe}\,\kappa. \tag{C4}$$

We shall assume that the dense phase has density $\phi_{\rm d} \approx 1$.

Mass conservation—There are $N_{\rm tot} = \phi A$ particles in the simulation box, A being the simulation box area. Let there be $N_{\rm d} = \phi_{\rm d}A_{\rm d} \approx A_{\rm d}$ particles in the dense phase and $N_{\rm g} = \phi_{\rm g}(A - A_{\rm d})$ particles in the gas phase, where $A_{\rm d}$ is the area of the simulation box taken up by the dense phase. Mass conservation implies

$$A_{\rm d} + \phi_{\rm g}(A - A_{\rm d}) = \phi A. \tag{C5}$$

We use Eq. (C4) to eliminate $\phi_{\rm g} = (\mathrm{Pe}\,\kappa)^{-1}$ from Eq. (C5). We eliminate A and $A_{\rm d}$ from the same equation in favor of $f \equiv A_{\rm d}/(\phi A)$, the fraction of particles in the solid phase. We get

$$f = \frac{\mathrm{Pe}\,\kappa - 1/\phi}{\mathrm{Pe}\,\kappa - 1}. \tag{C6}$$

From Eq. (C6), we see that phase separation is only possible if $\mathrm{Pe} > 1/(\kappa\phi)$. Thus infinite Pe is required to induce phase separation in the limit of vanishing packing fraction. For large Pe, we have $f \to 1$, i.e., all particles will be in the dense phase. [In the limit of large v_+ we have $\kappa \to (1-\mathrm{e}^{-4})/4 \approx 0.245$.]

The contour $f = 1/2$ from Eq. (C6) is plotted against simulation data in Fig. 2. The correspondence shown there indicates that a flux-balance argument can describe the essence of motility-induced phase separation for on-lattice active matter, just as it does off lattice.

APPENDIX D: SUPPLEMENTAL FIGURES

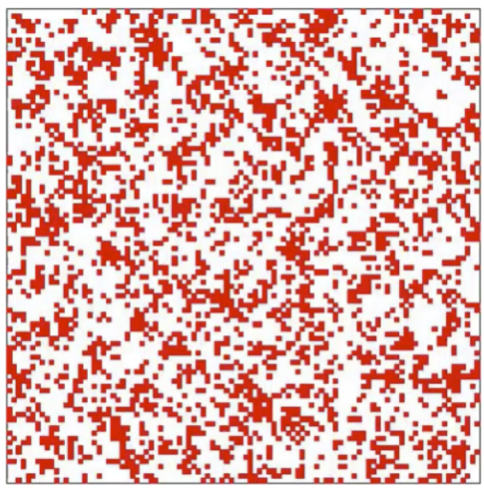

FIG. 6. Movie of phase separation and cluster dynamics. Multimedia view: https://doi.org/10.1063/1.5023403.1

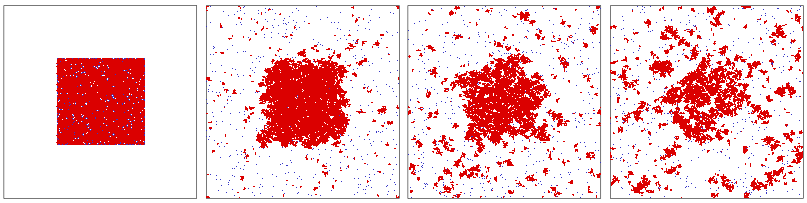

FIG. 7. When lateral motion is not possible (here $v_- = v_0 = 0$), phase separation does not occur. A pre-built compact cluster of particles dissolves into several smaller ones. ($v_+ = 25$, $\phi = 1/5$). When lateral motion is restored, phase separation is made possible; see Fig. 1 of the main text.

[1] J. Tailleur and M. Cates, Phys. Rev. Lett. **100**, 218103 (2008).
[2] S. Weitz, A. Deutsch, and F. Peruani, Phys. Rev. E **92**, 012322 (2015).
[3] A. Baskaran and M. C. Marchetti, Proc. Natl. Acad. Sci. U. S. A. **106**, 15567 (2009).
[4] F. Peruani, J. Starruß, V. Jakovljevic, L. Søgaard-Andersen, A. Deutsch, and M. Bär, Phys. Rev. Lett. **108**, 098102 (2012).
[5] J. Barré, R. Chétrite, M. Muratori, and F. Peruani, J. Stat. Phys. **158**, 589 (2015).
[6] F. Peruani, T. Klauss, A. Deutsch, and A. Voss-Boehme, Phys. Rev. Lett. **106**, 128101 (2011).
[7] S. Ramaswamy, Annu. Rev. Condens. Matter Phys. **1**, 323 (2010).
[8] P. Romanczuk, M. Bär, W. Ebeling, B. Lindner, and L. Schimansky-Geier, Eur. Phys. J.: Spec. Top. **202**, 1 (2012).
[9] G. S. Redner, M. F. Hagan, and A. Baskaran, Phys. Rev. Lett. **110**, 055701 (2013).
[10] M. C. Marchetti, J. Joanny, S. Ramaswamy, T. Liverpool, J. Prost, M. Rao, and R. A. Simha, Rev. Mod. Phys. **85**, 1143 (2013).
[11] I. Buttinoni, J. Bialké, F. Kümmel, H. Löwen, C. Bechinger, and T. Speck, Phys. Rev. Lett. **110**, 238301 (2013).
[12] J. Stenhammar, A. Tiribocchi, R. J. Allen, D. Marenduzzo, and M. E. Cates, Phys. Rev. Lett. **111**, 145702 (2013).
[13] J. Yeomans, D. Pushkin, and H. Shum, Eur. Phys. J.: Spec. Top. **223**, 1771 (2014).
[14] M. E. Cates and J. Tailleur, Annu. Rev. Condens. Matter Phys. **6**, 219 (2015).
[15] A. M. Menzel, Phys. Rep. **554**, 1 (2015).
[16] C. Bechinger, R. D. Leonardo, H. Lowen, C. Reichhardt, G. Volpe, and G. Volpe, Rev. Mod. Phys. **88**, 045006 (2016).
[17] V. Narayan, S. Ramaswamy, and N. Menon, Science **317**, 105 (2007).
[18] M. B. Wan, C. J. O. Reichhardt, Z. Nussinov, and C. Reichhardt, Phys. Rev. Lett. **101**, 018102 (2008).
[19] L. Angelani, R. D. Leonardo, and G. Ruocco, Phys. Rev. Lett. **102**, 048104 (2009).
[20] R. Di Leonardo, L. Angelani, D. Dell'Arciprete, G. Ruocco, V. Iebba, S. Schippa, M. P. Conte, F. Mecarini, F. De Angelis, and E. Di Fabrizio, Proc. Natl. Acad. Sci. U. S. A. **107**, 9541 (2010).
[21] L. Angelani and R. Di Leonardo, New J. Phys. **12**, 113017 (2010).
[22] P. K. Ghosh, V. R. Misko, F. Marchesoni, and F. Nori, Phys. Rev. Lett. **110**, 268301 (2013).
[23] A. Kaiser, A. Peshkov, A. Sokolov, B. ten Hagen, H. Lowen, and I. S. Aronson, Phys. Rev. Lett. **112**, 158101 (2014).
[24] S. A. Mallory, C. Valeriani, and A. Cacciuto, Phys. Rev. E **90**, 032309 (2014).
[25] J. Bialké, J. T. Siebert, H. Löwen, and T. Speck, Phys. Rev. Lett. **115**, 098301 (2015).
[26] A. Thompson, J. Tailleur, M. Cates, and R. Blythe, J. Stat. Mech.: Theory Exp. **2011**, P02029.
[27] K. R. Pilkiewicz and J. D. Eaves, Phys. Rev. E **89**, 012718 (2014).
[28] Y. Fily and M. C. Marchetti, Phys. Rev. Lett. **108**, 235702 (2012).
[29] J. Palacci, S. Sacanna, A. P. Steinberg, D. J. Pine, and P. M. Chaikin, Science **339**, 936 (2013).
[30] B. M. Mognetti, A. Saric, S. Angioletti-Uberti, A. Cacciuto, C. Valeriani, and D. Frenkel, Phys. Rev. Lett. **111**, 245702 (2013).
[31] T. Speck, J. Bialké, A. M. Menzel, and H. Löwen, Phys. Rev. Lett. **112**, 218304 (2014).
[32] J. Stenhammar, R. Wittkowski, D. Marenduzzo, and M. E. Cates, Phys. Rev. Lett. **114**, 018301 (2015).
[33] G. S. Redner, C. G. Wagner, A. Baskaran, and M. F. Hagan, Phys. Rev. Lett. **117**, 148002 (2016).
[34] F. Peruani, L. Schimansky-Geier, and M. Bär, Eur. Phys. J.: Spec. Top. **191**, 173 (2010).
[35] R. Dickman, New J. Phys. **18**, 043034 (2016).
[36] R. J. Baxter, *Exactly Solved Models in Statistical Mechanics* (Academic Press, 1982).
[37] J. J. Binney, N. Dowrick, A. Fisher, and M. Newman, *The Theory of Critical Phenomena: An Introduction to the Renormalization Group* (Oxford University Press, Inc., 1992).
[38] D. Chandler, *Introduction to Modern Statistical Mechanics* (Oxford University Press, 1987), ISBN-10: 0195042778, ISBN-13: 9780195042771.
[39] K. Binder, in *Monte Carlo Methods in Statistical Physics* (Springer, 1986), pp. 1–45.
[40] S. Katz, J. L. Lebowitz, and H. Spohn, J. Stat. Phys. **34**, 497 (1984).
[41] R. Zia, J. Stat. Phys. **138**, 20 (2010).
[42] A. P. Solon and J. Tailleur, Phys. Rev. E **92**, 042119 (2015).
[43] A. Solon and J. Tailleur, Phys. Rev. Lett. **111**, 078101 (2013).
[44] N. Sepúlveda and R. Soto, Phys. Rev. Lett. **119**, 078001 (2017).
[45] R. Soto and R. Golestanian, Phys. Rev. E **89**, 012706 (2014).
[46] K. Klymko, P. L. Geissler, J. P. Garrahan, and S. Whitelam, Phys. Rev. E **97**, 032123 (2018).
[47] S. Whitelam, Phys. Rev. E **97**, 032122 (2018).
[48] D. Gillespie, J. Comput. Phys. **22**, 403 (2005).
[49] D. Ruelle, *Thermodynamic Formalism: The Mathematical Structure of Equilibrium Statistical Mechanics* (Cambridge University Press, 2004).
[50] J. P. Garrahan, R. L. Jack, V. Lecomte, E. Pitard, K. van Duijvendijk, and F. van Wijland, Phys. Rev. Lett. **98**, 195702 (2007).
[51] V. Lecomte, C. Appert-Rolland, and F. van Wijland, J. Stat. Phys. **127**, 51 (2007).
[52] J. P. Garrahan, R. L. Jack, V. Lecomte, E. Pitard, K. van Duijvendijk, and F. van Wijland, J. Phys. A: Math. Theor. **42**, 075007 (2009).
[53] L. O. Hedges, R. L. Jack, J. P. Garrahan, and D. Chandler, Science **323**, 1309 (2009).
[54] H. Touchette, Phys. Rep. **478**, 1 (2009).
[55] C. Maes and K. Netočnỳ, Europhys. Lett. **82**, 30003 (2008).
[56] C. Giardina, J. Kurchan, V. Lecomte, and J. Tailleur, J. Stat. Phys. **145**, 787 (2011).
[57] V. Lecomte and J. Tailleur, J. Stat. Mech.: Theory Exp. **2007**, P03004.
[58] T. Nemoto and S.-i. Sasa, Phys. Rev. Lett. **112**, 090602 (2014).
[59] R. L. Jack and P. Sollich, Eur. Phys. J.: Spec. Top. **224**, 2351 (2015).
[60] T. Nemoto, F. Bouchet, R. L. Jack, and V. Lecomte, Phys. Rev. E **93**, 062123 (2016).
[61] A. A. Budini, R. M. Turner, and J. P. Garrahan, J. Stat. Mech.: Theory Exp. **2014**, P03012.
[62] R. L. Jack, I. R. Thompson, and P. Sollich, Phys. Rev. Lett. **114**, 060601 (2015).
[63] The linguistically unfortunate result is that making passive particles ($v_+ = 1$) active ($v_+ > 1$) reduces their emergent activity (ν decreases).
[64] A. S. Mey, P. L. Geissler, and J. P. Garrahan, Phys. Rev. E **89**, 032109 (2014).
[65] B. ten Hagen, S. van Teeffelen, and H. Löwen, J. Phys.: Condens. Matter **23**, 194119 (2011).
[66] J. R. Howse, R. A. Jones, A. J. Ryan, T. Gough, R. Vafabakhsh, and R. Golestanian, Phys. Rev. Lett. **99**, 048102 (2007).
[67] T. Glanz and H. Löwen, J. Phys.: Condens. Matter **24**, 464114 (2012).
[68] H. Tanaka, A. A. Lee, and M. P. Brenner, Phys. Rev. Fluids **2**, 043103 (2017).